Proceedings in Manufacturing Systems, Volume 17, Issue 3, 2022, 103-108 ISSN 2067-9238

STIFFNESS PARAMETERS EVALUATION OF PANELS HINGE FOR CARDSAT MICROSATELLITE DEPLOYMENT

Claudiu BÎŞU[1,*], Tudor George ALEXANDRU[2], Cristina PUPĂZĂ[3], Luminiţa GEORGESCU[4]

[1)] Assoc. Prof., PhD, Robots and Manufacturing Systems Department, University "Politehnica" of Bucharest, Romania
[2)] Lecturer, PhD, Robots and Manufacturing Systems Department, University "Politehnica" of Bucharest, Romania
[3)] Prof., PhD, Robots and Manufacturing Systems Department, University "Politehnica" of Bucharest, Romania
[4)] PhD Msc. Eng., Faculty of Industrial Engineering and Robotics, University "Politehnica" of Bucharest, Romania

Abstract: *Self-opening panels are employed in the design of small satellites for extending their mission capabilities. Such solutions comprise an array of mechanical or electromechanically actuated joints that can deploy solar panels, communication antennas or scientific instruments in their operating position. Various sizing methodologies are depicted throughout the literature for deciding the optimal parameters of the deployment mechanisms. However, an accurate description of the loads that act on self-opening panels can only be achieved with the support of experimental and simulation procedures. The present paper studies the stiffness characteristics of laminar spring type joints in a new approach. Experiments are conducted on a laboratory scale prototype. An incremental pressure is applied normal to the spring surface. A displacement sensor captures the radial deflection of the specimen. Afterwards, a FEM simulation model is developed by taking into account the geometric and material characteristics of the assembly. The same loads and boundary conditions that are employed in the test platform are considered for completing the numeric study. A good match was noticed between the stiffness characteristics derived by means of experiments and simulations. The results achieved can be further used for replicating the linear elastic behavior of MAEVA joints.*

Key words: *small satellite, self-opening, laminar spring, stiffness, FEM simulation.*

¶

1. INTRODUCTION

In the past decades, small satellites have emerged as a cost-effective alternative to larger and more complex spacecraft [1, 2, 3]. Such solutions are based on modular design concepts and can be employed for a wide variety of scientific and communication missions that take place in the Low Earth Orbit (LEO) [4].

The custom-tailoring of small satellites is completed with the support of self-opening panels [5]. Such deployable mechanisms ensure the opening and locking of power, instrumentation or other scientific equipment without external assistance or control [6]. The actuating mechanisms used in the design of such solutions include hinge, slotted joint, ball and socket, universal joints [7].

The MAEVA (Mechanical Assembly and EVA Deployment) is a type of joint used in the design of self-opening panels for small satellites [8]. Its design comprises a hinge-based mechanism that allows the rotational motion of the panel during the deployment or stowing cycles. The MAEVA joint is designed to be simple, lightweight, and reliable, with minimal moving parts, making it suitable for use in the harsh environment of the LEO.

The existing literature focuses on the experimental evaluation of the MAEVA joints [9 and 10]. On the other hand, a wide variety of research papers depict numerical simulation models that can be employed for deciding the optimal parameters of such mechanisms [11 and 12].

The present paper studies the stiffness characteristics of a laboratory scale MAEVA joint by experimental and numerical means.

In the first stage, a laboratory scale prototype is developed, comprising a high carbon steel laminar spring that has a free end. The column of a CNC machine tool is used to exert pressure on the top side of the hinge. This objective is completed by gradually incrementing the displacement on the *Z*-axis.

The force reaction due to this motion is captured with the support of a digital dynamometer. On the other hand, a displacement sensor is included to measure the radial deflection of the specimen.

A FEM simulation model is developed in the next stage. The geometric, material and load characteristics of the studied joint are taken into account. Stiffness calculations are completed based on the deformation of the specimen. A good match was noticed between the stiffness characteristics derived by experimental and simulation means.

2. THE STUDIED ASSEMBLY

The MAEVA joint in discussion is part of a modular design small satellite. Its primary structure comprises rectangular aluminum frames (Fig. 1).

[*] Corresponding author: 313 Splaiul Independenţei, 060042, Bucharest, Romania
Tel.: +40214029369;
E-mail addresses: *cfbisu@gmail.com* (C. Bîşu)

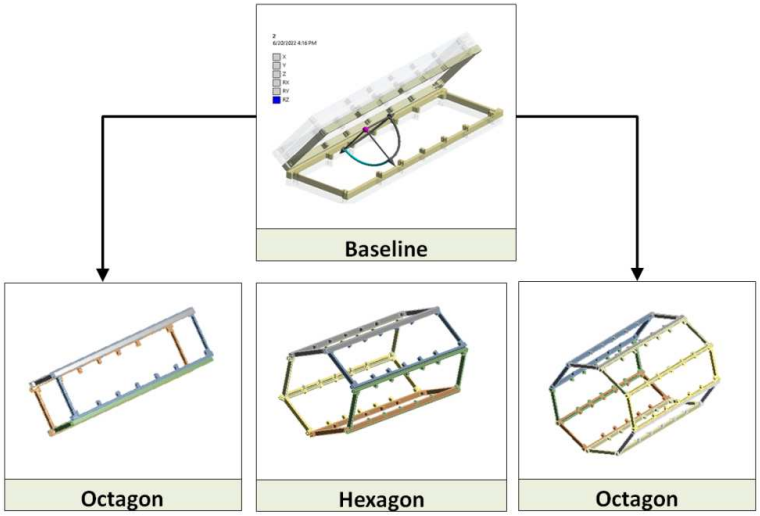

Fig. 1. Multiple configurations of the self-opening panels.

The assembly can achieve multiple opening configurations based on the payload requirements of the stakeholder:

- Quadrilateral: includes 4 self-opening panels, 3 joint arrays with an opening angle of 90 °.
- Pentagon: includes 5 self-opening panels, 4 joint arrays with an opening angle of 108 °.
- Hexagon: includes 6 self-opening panels, 5 joint arrays with an opening angle of 120 °.
- Heptagon: includes 7 self-opening panels, 6 joint arrays with an opening angle of 128.57 °.
- Octagon: includes 8 self-opening panels, 7 joint arrays with an opening angle of 135 °.

From this perspective, the evaluation of the stiffness parameters for a single joint can be completed based on D'Alambert principle:

$$[M]\cdot\{\ddot{u}\}+[C]\cdot\{\dot{u}\}+[K]\cdot\{u\}=\{f(t)\}, \tag{1}$$

where: f corresponds to the sum of all forces incident to the structure, u the displacement of the structure and its first and second order derivatives are the velocity and the acceleration. [**M**], [**C**] and [**K**] are the mass, damping and stiffness matrices.

In case of multiple joints the stiffness of the self-opening panels can be evaluated based on:

$$\frac{1}{K_o}=\frac{1}{K_{1-2}}+\frac{1}{K_{2-3}}+\frac{1}{K_{3-4}}+\ldots+\frac{1}{K_{(n-1)-(n)}}. \tag{2}$$

A graphical representation of the calculation methodology is depicted in Fig. 2 for a single self-opening panel assembly.

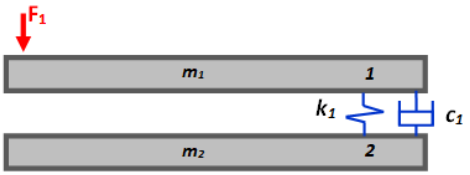

Fig. 2. The configurations of the self-opening panels.

3. THE PROPOSED APPROACH

The proposed approach (Fig. 3) comprises two layers of abstraction: the experimental and simulation layers.

3.1. The experimental environment

A laboratory scale MAEVA joint is developed by employing a laminar spring and two spacers which will serve as a fixed support. The top surface of the spring is subjected to radial loads which are induced by the displacement of a machine tool spindle. A test pin is installed in the tool holder for ensuring the contact between the spindle and the spring. The measurement of the reaction force is completed with the support of a digital dynamometer. On the other hand, the deflection magnitude is captured by means of a displacement sensor. The experimental values are stored on an acquisition PC.

In case of laminar springs, the bending stiffness depends on the material properties, geometry and the orientation of the applied load.

Assuming a free-end configuration with a uniform pressure that is exerted on the plate, the x component of stress can be evaluated as [13]:

$$\sigma_x \max=\frac{3qa^2}{h^2}, \tag{3}$$

where: q – the magnitude of the uniformly distributed load, a – length of the plate from the fixed to the free end and h the thickness of the plate.

$$\sigma_y \max=\nu\cdot\frac{3qa^2}{h^2}, \tag{4}$$

where: ν – the Poisson's ratio of the material.

The equivalent von Mises stress is:

$$\sigma_{vM} \max=\frac{3qa^2}{h^2}\cdot\sqrt{1+\nu^2-\nu}, \tag{5}$$

where P – the applied bending load [N].

Thus, the maximum deflection of the plate can be derived as:

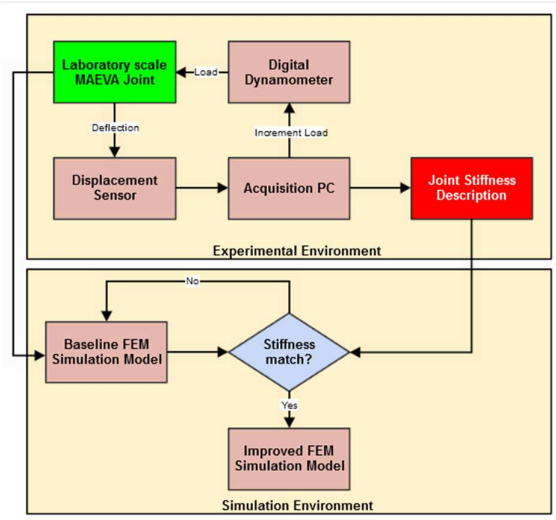

Fig. 3. A schematic representation of the proposed approach.

$$\delta_{\max} = \frac{3 \cdot \left(1 - \nu^2\right) \cdot q \cdot a^4}{2Eh^3}. \quad (6)$$

where: E – Modulus of elasticity of the material.

3.2. The simulation environment

The stiffness characteristics of the joint are further required for simulating the behavior of the self-opening panels. Different operational scenarios must be evaluated prior to the physical testing of the small satellite prototype.

This stage is usually completed with the support of FEM software. Examples include: the transient structural analysis of the deployable mechanism, the coupled thermal and mechanical analysis for preventing the failure of the joint or the modal analysis for identifying the natural frequencies of the entire assembly.

From this perspective, a simplified representation of the MAEVA joint is required.

The equations that express the balance of forces acting on the element can be written as [14]:

$$\nabla\sigma + f = 0. \quad (7)$$

The constitutive equation which describes the relationship between stress and strain can be expressed as:

$$\{\sigma\} = [D] \cdot \{\varepsilon\}, \quad (8)$$

where: D – the elasticity matrix and ε – strain tensor.

The displacement can be derived from the strain-displacement equation:

$$\{\varepsilon\} = [B] \cdot \{u\}, \quad (9)$$

where: B – the strain-displacement matrix and u – displacement vector.

4. EXPERIMENTAL RESULTS

Figure 4,*a* depicts the experimental setup while Figure 4,*b* shows the boundary conditions and the load application method.

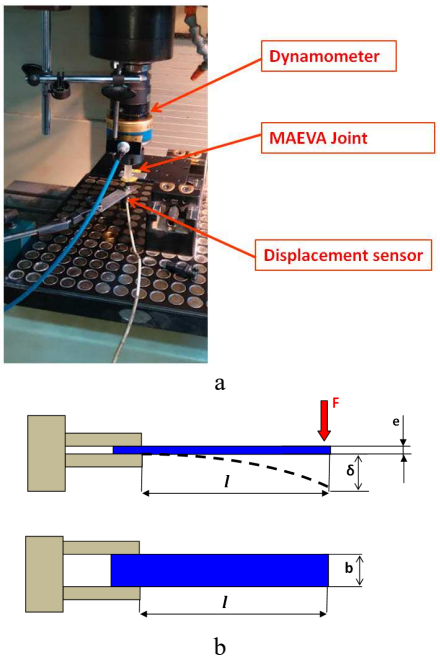

Fig. 4. The experimental platform: *a* – the main components; *b* – the load application method.

The geometric parameters of the laminar spring are: spring length l = 19 mm, spring width b = 25 mm and spring thickness e = 0.15 mm.

The force is measured by a 9125 A Kistler dynamometer while the displacement is determined by a displacement sensor. It allowed the measurement of two components: axial force F_z and axial torque M_z. Regarding the force measurement, the dynamometer offers three measurement ranges: first range 3000 N...3000 N, second range −1000 N...1000 N and third range −300 N...300 N. The sensitivity for the third range is 3.032 mV/N. The displacement is captured by the Bently Nevada 3300 Proximitor sensor, having the sensitivity of 7.87 V/mm, a measurement range of 5 mm and the recommended gap setting of 1.27 mm.

The material properties of the laminar spring are depicted in Table 1 [15].

Table 1

Material properties of the studied spring configuration

Material type	Modulus of Elasticity (MPa)	Poisson Ratio	Density (Kg/m^3)
High carbon steel alloy	$2 \cdot 10^5$	0.3	7800

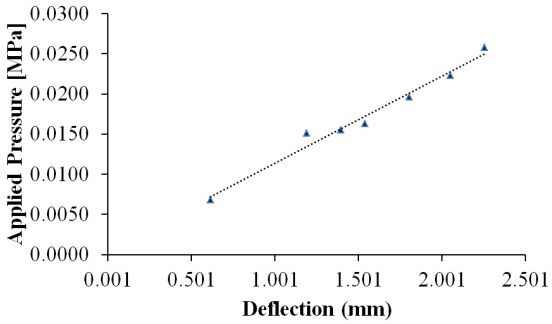

Fig. 5. Experimental results.

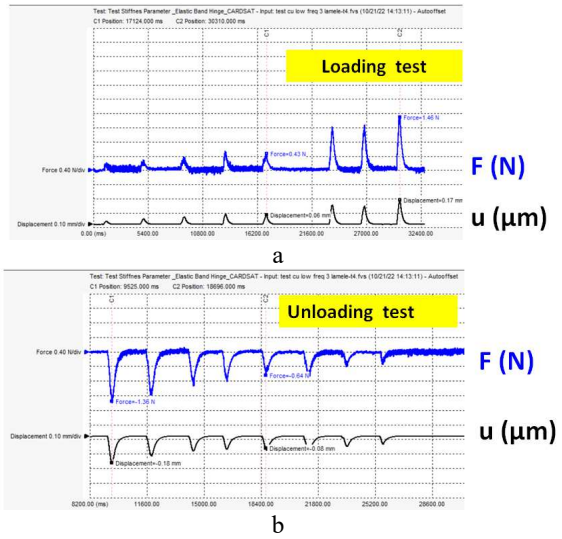

Fig. 6. Experimentally determined spring displacement: *a* – loading cycles; *b* – unloading cycles.

Figure 5 represents the relationship between the applied pressure and the displacement of the spring.

The values were derived from the loading and unloading test cycles, depicted in Figure 6,*a* and *b*.

A power function can be employed to determine the slope of the experimental data:

$$\delta = 0.589 \cdot F^{0.74}, \quad (10)$$

where: F – the load applied, the coefficient value is 0.589 and the exponent is 0.74.

5. SIMULATION RESULTS

5.1. The initial simulation model

The simulation model was developed in LISA Finite Element analysis package [16].

Information regarding the type of analysis and the modeling approach is depicted in Table 2.

Table 2

Material properties of the studied spring configuration

Analysis type	Modeling approach	Element type	Material model
Static	3D Shell	4 Node Quad	Isotropic elasticity

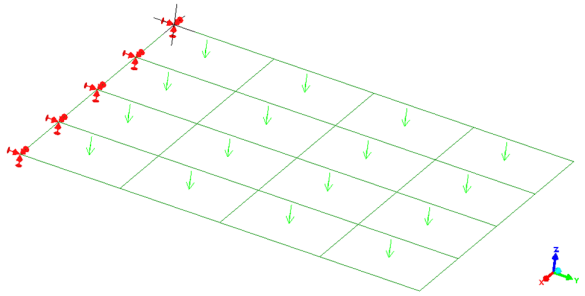

Fig. 7. Loads and Boundary conditions.

Table 3

Material properties of the studied spring configuration

Load applied [N]	Experimental deflection (mm)	Simulation deflection (mm)
0.61	0.42	0.41
1.19	0.64	0.80
1.39	0.7	0.94
1.54	0.8	1.04
1.80	0.96	1.21
2.05	1.1	1.37
2.25	1.3	1.51

The analysis type employed is a static one, given the equilibrium state of the structure and the applied load. A 3D shell simulation approach is considered due to the fact that the thickness of the specimen is significantly smaller than its other dimensions. 4 Node quadrangular elements are used for defining the mesh. Uniform thickness rectangular flat plate geometry is considered. The material properties are defined as linear elastic. In this regard, only the modulus of elasticity and Poisson's ratio are employed in the analysis. Figure 7 illustrates the simulation model and its boundary conditions.

The loads are applied with respect to the experimental procedure from Fig. 5. On the other hand, the same boundary conditions are considered.

Table 3 depicts the Z axis displacement of the specimen side-by-side with the deflection derived by means of experiments.

In this case, the coefficient value of the simulation power function is 0.673 (ε = 12%) while the exponent is 0.99 (ε = 17%).

Figure 8 depicts the bending displacement fringe for the first case.

This behavior can be explained by the geometry of the MAEVA joint. In this case, the lamellar spring has a rectangular curved cross section. This design allows a wider range of movement and flexibility compared to the flat plate. Thus, when the assembly is subjected to bending loads, a more gradual distribution of stress and

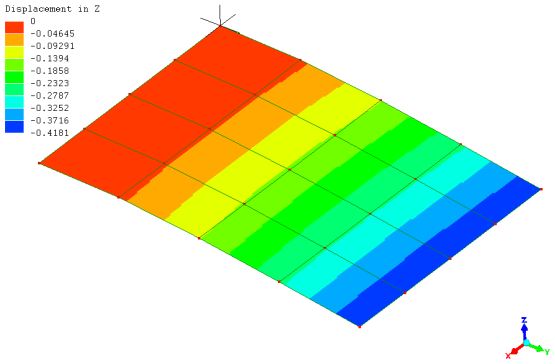

Fig. 8. Displacement fringe of the flat plate geometry.

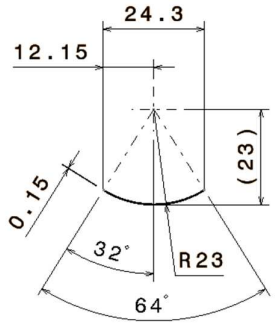

Fig. 9. Curved surface laminar spring.

strain occurs along the length of the spring. From this perspective, repeated opening-closing cycles of the joint can be completed without the risk of fatigue damage. On the other hand, the magnitude of the pressure load that acts on the specimen is considered constant in any location of the top surface.

To overcome such issues, the real geometry must be taken into account. Figure 9 represents the drawing of the of the laminar spring cross-section.

5.2. The improved simulation model

The actual geometry of the specimen is taken into account in the FEM simulation model.

When a curved surface is subjected to bending loads, it exhibits two types of stresses: compressive stress on the concave side and tensile stress on the convex side. In the case of a flat plate, these stresses are distributed evenly over the entire surface area, causing a uniform displacement state. However, in the case of curved plates, the stresses are concentrated towards its center, leading to a smaller region of deformation. This effect is caused by the radius of the curvature which is smaller at the center than at the edges. Thus, curved surface laminar springs achieve superior bending stiffness than compared to flat plate ones.

Table 4 depicts the differences between the experimental and simulation model for the curved surface geometry.

Figure 10 shows the displacement fringe achieved for the first set of values.

Table 4

Material properties of the studied spring configuration

Load applied [N]	Experimental deflection (mm)	Simulation deflection (mm)
0.61	0.42	0.02
1.19	0.64	0.04
1.39	0.7	0.05
1.54	0.8	0.06
1.80	0.96	0.07
2.05	1.1	0.07
2.25	1.3	0.08

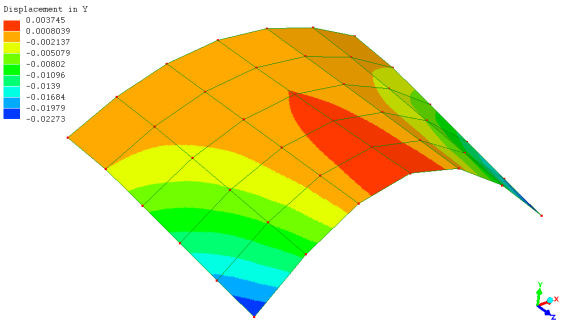

Fig. 10. Displacement fringe of the curved surface geometry.

The margin of errors achieved in this case exceeds the ones depicted in the initial simulation model (ε = 95%). Thus, a different simulation approach is required.

One important aspect which is neglected in the curved surface simulation model is the fact that the assembly conditions of the joint impose a compressive load on the top of the spring. Thus, the bending stiffness of the curved surface plate will be different in the deformed shape compared to the undeformed one due to changes in the plate's curvature.

The moment of inertia of a curved surface plate is directly proportional to the square of its curvature radius. As the radius changes under the effect of the load, the moment of inertia also changes, which in turn affects the bending stiffness of the plate. Thus, the distribution of stresses also changes, which affects the overall strength and stiffness of the joint.

This pre-stress effect is taken into account in the simulation model by dividing the analysis in two steps:

Step 1: a flexible displacement condition is imposed on the left and right edges of the specimen. All other degrees of freedom are restrained on one of the edges which describe the height.

Step 2: the same loads depicted in the previous studies are considered.

Table 5 points out the differences between the experimental and simulation model for the pre-stress curved surface geometry.

In this case, the coefficient value of the simulation power function is 0.58 (ε = 5.15%) while the fixed variable is 0.71 (ε = 3.95%).

Note that the simulation deflection is derived by subtracting the maximum negative displacement of the structure that occurs in the initial and final load steps. For example, the negative *Y* component displacement that takes place due to the pre-stress effect is 0.69 mm. After

Table 5

Material properties of the studied spring configuration

Load applied [N]	Experimental deflection (mm)	Simulation deflection (mm)
0.61	0.42	0.41
1.19	0.64	0.60
1.39	0.7	0.68
1.54	0.8	0.76
1.80	0.96	0.91
2.05	1.1	1.02
2.25	1.3	1.24

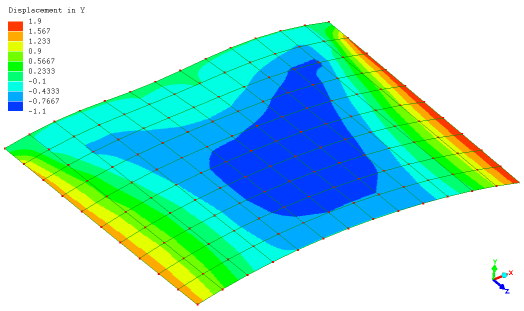

Fig. 11. Displacement fringe of the curved surface geometry considering the pre-stress effect.

the bending pressure is applied, the new displacement value reaches −1.1 mm. Thus, the calculated simulation deflection is 0.41 mm, which matches the experimentally derived one (Fig. 11).

6. CONCLUSIONS

The present paper proposes a new approach for identifying the stiffness of MAEVA joints. Experiments are carried out by considering a laboratory platform. The displacement of the specimen is evaluated under varying bending loads. A machine tool Z-axis is used for this purpose. Loading and unloading cycles are considered. A digital dynamometer measures the reaction force. The deflection of the specimen is captured by means of a displacement sensor. A 3D shell simulation strategy is proposed, assuming a linear elastic behavior of the material. In the initial stage, the geometry of the laminar spring is approximated as a flat plate. The experimentally derived values match the simulation ones only for the first load cycle. Afterward, errors in excess of 34% can be noticed. To overcome such issues, the shape of the shell mesh is adjusted to match the curvature of the sample. The simulation results prove an excessive increase of the bending stiffness. In this case, the difference between the experimental vs. simulation deflection values exceeds 95%. In the final stage, the pre-stress that is imposed by the assembly conditions is taken into account. A flexible displacement boundary condition is defined in the first load step, while the bending pressure which acts on the specimen is activated in the second step. A good match was achieved between the experimental and simulation values, the errors reaching less than 5.15%. Thus, the approach can successfully be employed for evaluating the bending stiffness of MAEVA joints.

Acknowledgements: This work was supported by the 1st priority axis of "The Competitiveness Operational Program" [ID / Cod MySMIS: 120353] in the framework of "Advanced Technologies for Manufacturing and Testing of Advanced Materials in the Aerospace Domain", Contract number [402/390078/24.12.2021].

REFERENCES

[1] M. Sweeting, *Modern Small Satellites,* Changing the Economics of Space, February 2018, Proceedings of the IEEE, Vol. 106 (3), pp. 343-361, DOI: https://doi.org/10.1109/JPROC.2018.2806218

[2] P. Allen, J. Wickham-Eade, M. Trichas, *The potential of small satellites for scientific and astronomical discovery*, Nature Astronomy, Vol. 4, Nov. 2020, pp.1039-1042.

[3] S. Malisuwan, B. Kanchanarat, *Small Satellites for Low-Cost Space Access: Launch, Deployment, Integration, and In-Space Logistics*. American Journal of Industrial and Business Management, 12, 2022, pp. 1480-1497.

[4] Kopacz, J.R, Herschitz, R., Roney, J. - Small satellites an overview and assessment, Acta Astronautica, ISSN 0094-5765, Vol. 170, 2020, pp. 93–105.

[5] S. Bhattarai, J-S Go, H. Kim, H-U Oh, *Development of a Novel Deployable Solar Panel and Mechanism for 6U CubeSat of STEP Cube Lab-II*. Aerospace 2021, 8, pp. 64. https://doi.org/10.3390/ aerospace8030064

[6] J. Fajardo, A.A. Lidke, S.A. Bendoukha, *Design, implementation, and operation of a small satellite mission to explore the space weather effects in LEO*, *Aerospace* 6.10, 2019, pp. 108.

[7] X. Zhao, C. Zhao, J. Li, Y. Guan, S. Chen, L. Zhang, Research on Design, Simulation, and Experiment of Separation Mechanism for Micro-Nano Satellites, *Applied Sciences* 12.12, 2022, pp. 5997.

[8] D.Y. Kim, H.S. Choi, J.H. Lim, K.W. Kim, J. Jeong, *Experimental and numerical investigation of solar panels deployment with tape spring hinges having nonlinear hysteresis with friction compensation,* Applied Sciences 10.21 (2020): 7902.

[9] F. Dewalque, C. Schwartz, V. Denoël, J-L. Croisier, B. Forthomme, O. Brüls, *Experimental and numerical investigation of the nonlinear dynamics of compliant mechanisms for deployable structures*, Mechanical Systems and Signal Processing, ISSN 0888-3270, Volume 101, 2018, pp. 1–25, https://doi.org/10.1016/j.ymssp.2017.08.006.

[10] JW Jeong, Yi Yoo, DK Shin, JH Lim, *A novel tape spring hinge mechanism for quasi-static deployment of a satellite deployable using shape memory alloy*, Review of Scientific Instruments, 85.2, 2014, p. 025001.

[11] H. Ye, Y. Zang, Q. Yang, B. Zhang, *Quasi-static analysis and multi-objective optimization for tape spring hinge,* Structural and Multidisciplinary Optimization, 60, 2019, pp. 2417–2430.

[12] Z. Elbara, C.S. Patmont, Th. Fritz, *Design and characterization of a spring steel hinge for deployable CubeSat structures*. Journal of Small Satellites, 5.1, 2016, pp. 407–418.

[13] M. Banasiak, K. Grossman, & M. Trombski, *Zbiór zadań z wytrzymałości materiałów*, Wydawnictwo Naukowe PWN, Poland, 1998.

[14] M. Okereke, S. Keates, *Finite element applications. A Practical Guide to the FEM Process*, Springer International Publishing AG, Springer, Switzerland, 2018.

[15] MATWEB, Material Property Data, https://www.matweb.com, accessed: 2022-10-12.

[16] LISA V. 8.0.0, Free FEA, https://lisafea.com, accessed: 2022-10-12.